Features of the extreme events observed in an all-solid-state laser with a saturable absorber

Carlos R. Bonazzola,[1,2,*] Alejandro A. Hnilo,[1] Marcelo G. Kovalsky,[1] and Jorge R. Tredicce[2,3]

[1]*Centro de Investigaciones y Aplicaciones (CEILAP), UNIDEF (MINDEF-CONICET), J.B. de La Salle 4397, 1603 Villa Martelli, Argentina*

[2]*Departamento de Física, FCEN - Universidad de Buenos Aires, Ciudad Universitaria Pabellón 1, 1428 Buenos Aires, Argentina*

[3]*Pole Pluridisciplinaire de la Matière et l'Environment, Université de la Nouvelle Calédonie, EA3325 Nouméa, Nouvelle Calédonie, France*

(Received 15 July 2015; published 6 November 2015)

Extreme events in the form of pulses of extraordinary intensity (sometimes also called optical rogue waves) are easily observed in the chaotic regime of an all-solid-state laser with a saturable absorber if the Fresnel number of the cavity is high. This result suggests that the nonlinear interaction among transverse modes is an essential ingredient in the formation of extreme events in this type of laser, but there is no theoretical description of the phenomenon yet. We report here a set of experimental results on the regularities of these extreme events in order to provide a basis for the development of such a description. Among these results, we point out here (i) the decay of the correlation across the transversal section of the laser beam, and (ii) the appearance of extreme events even if the time elapsed since the previous pulse is relatively short (in terms of the average interpulse time interval), which indicates the existence of some unknown mechanism of energy storage. We hypothesize that this mechanism is related to the imperfect depletion of the gain by some of the transversal modes. We also present evidence in support of this hypothesis.

DOI: 10.1103/PhysRevA.92.053816 PACS number(s): 42.60.Mi, 42.65.Sf, 05.45.Tp

I. INTRODUCTION

In recent years there has been a growing interest in extreme events (EEs) in various disciplines [1]. The first reliable measurements of freak or rogue waves (i.e., unexpectedly large oceanic waves, as high as 30 m from crest to trough) in the beginning of the 1990s were followed by intensive research on what had previously been considered a near-mythological phenomenon. In 2007 Solli *et al.* introduced the concept of optical rogue waves to describe large fluctuations in the edge of the spectrum of the light generated by the propagation of seed pulses in a microstructured optical fiber, thus posing an analogy between the optical pulses and their oceanic counterparts [2]. The authors did so based, first, on the L-shaped statistics of the optical events (long-tailed distributions imply the existence of EEs that, although rare, are observed with non-negligible probability), and second, the theoretical approach they employed to describe the results of the experiment. This description is based on the nonlinear Schrödinger equation (used in this case to describe the propagation of pulses in the optical fiber). Since then, similar phenomena have been found and studied in a wide variety of optical systems under the broad denomination of optical rogue waves or EEs, meaning, roughly speaking, extreme fluctuations in the value of an optical field [3]. However, we must warn the reader that this does not imply, *a priori*, a common generation mechanism of these phenomena or even a common single definition. In fact, even in oceanography, where the term *rogue wave* was originally coined, a unified definition does not yet exist [4]. The task becomes more difficult when considering diverse physical systems beyond the oceans and analogies between these phenomena must be dealt with carefully. (A thorough discussion on this topic can be found in Ref. [3].) Regardless of their connection with their oceanic counterparts, optical EEs are intrinsically interesting. EEs had been observed in optical systems, but not recognized as such, earlier in the history of lasers [5–7]. They have been studied in extended optical systems (including a linear and a nonlinear experiment—a laser beam focused into a perturbed multimode glass fiber, and an optical cavity that uses a liquid-crystal light valve as nonlinear medium, respectively) [8], in optically injected semiconductor lasers [9–11], and in lasers with saturable absorbers, both *fast* (in a Kerr lens mode-locked laser) [12] and *slow* (in a passively Q-switched all-solid-state $Nd:YAG + Cr:YAG$ laser) [13]. For a comprehensive review, we refer the reader to [14]. In particular, we reported the existence of EEs in a system similar to the latter: a $Nd:YVO_4 + Cr:YAG$ laser [15], a device of a wide practical interest. We showed that EEs are observed in chaotic regimes with high dimension of embedding, high Fresnel number for the cavity, and complex spatial transverse patterns of the spot. The standard theoretical approach based on rate equations for a single mode [16] is able to describe many of the dynamical features of this system, but it does not predict the existence of EEs. This result suggests that interaction of transverse modes is a necessary condition for the formation of EEs in this system. One of the aims of this contribution is to provide further proof for this claim. Another goal is to perform a thorough exploration of the regimes in which EEs appear, and of the EEs themselves, to guide the theoretical modeling of the problem, as well as to outline key points that should be predicted by such a model. With these objectives in mind, we analyze some of the spatiotemporal features of the dynamics of these events. The understanding of the mechanism of formation of EEs in this system may conceivably lead to their control and, eventually, to useful applications.

In order to quantitatively define EEs, we adopt the criterion that the pulses with a peak intensity exceeding the mean by more than 4 times the standard deviation of the peak intensity distribution (4σ threshold) qualify as EEs. This criterion is somewhat arbitrary; however, we show later that it is appropriate not only because the events that fulfill it are among the highest in a particular regime of laser operation,

*Corresponding author: cbonazzola@gmail.com

but also because they exhibit peculiar dynamical features. Besides, we are specifically interested in those EEs appearing in regimes with long-tailed histograms, where EEs appear more frequently than in Gaussian distributions. In other words, we are interested in distributions with a kurtosis higher than 3.

This paper is organized as follows. Section II is devoted to experimental considerations: we describe the laser and the methods to record and analyze the time series (II A), as well as the setup to observe transversal coherence domains (II B) and the spatial correlation among different sections of the spot (II C). In Sec. III, we discuss the main experimental results, namely: (i) the plots of intensities in partial sections of the spot show that the EEs are not linked to a unique transverse pattern (III A 1); (ii) in the dynamical regimes with EEs, the two-point time correlation decays to zero at a distance nearly half the size of the spot, while in periodic regimes such decay is not observed (III A 2); (iii) the study of the time intervals between successive pulses suggests that the EEs occur in a relatively well-defined manifold in the phase space and, consequently, there is some hope to predict them (III B), a claim supported by the behavior of the peak intensity return maps (III C); and (iv) heterodyne interferograms indicate the existence of domains of transversal coherence, confirming the results of (i) (III D). Only a few time series out of many recorded and studied are shown in this paper as illustration. A diagram summarizing the main results for all the series where embedding dimension is able to be measured shows that the regimes with EEs are chaotic (i.e., with one positive Lyapunov exponent) or hyperchaotic (more than one positive Lyapunov exponent) with embedding dimension larger than 6, and that they have relatively complex transverse patterns (III E). In what follows, we assume the reader to be familiar with the essentials of self-Q-switching theory [17–19].

II. EXPERIMENTAL SETUP

A. The laser

The setup is shown in Fig. 1. The output of a 2-W (at 808 nm) cw laser diode is collimated by a gradient-index (GRIN) lens and focused down to a spot $\simeq$0.8 mm in diameter into a Nd : YVO_4 crystal, 1% doped and mounted on a water-cooled copper heat sink. The "external" face of the Nd : YVO_4 crystal has a high-reflection (HR) coating at 1064 nm in order to close the laser cavity and an antireflection (AR) coating at 808 nm in order to allow the pump radiation to enter the cavity. This is the standard coating for this type of crystals. The V-shaped laser cavity has a folding HR at 1064 nm concave mirror ($R = 100$ mm) and a plane output coupler (reflectivity 98% at 1064 nm). The operating wavelength of the laser is 1064 nm, linearly polarized. This radiation is separated from the pump radiation, when it is necessary, by the insertion of interferential filters (centered at 1064 nm, bandwidth 20 nm) before the detectors or camera. The mode size varies strongly between the mirrors, with the waist near the output coupler. The geometry of the cavity defines a Fresnel number $F \approx 10$. The average output power is measured with the power meter (PM) placed after the output

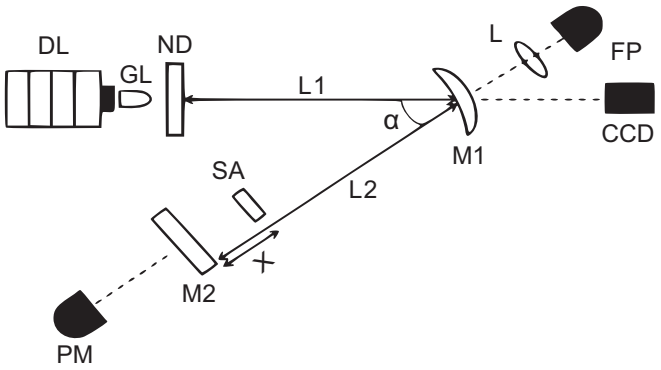

FIG. 1. Laser setup. LD: pump laser diode, 2 W cw at 808 nm; GL: GRIN lens; ND: Nd : YVO4 slab (active medium); M1: folding mirror ($R = 100$ mm); M2: output mirror (plane); SA: Cr : YAG crystal, transmission (unbleached) 90%; L: focusing lens; FP: fast photodiode; CCD: camera for recording spot images; PM: power meter, $\alpha = 20^\circ$; L1 = 130 mm; L2 = 70 mm. The position X of the SA is variable to obtain different dynamical regimes. The operating laser wavelength is 1064 nm.

coupler. A solid-state saturable absorber (Cr : YAG crystal, 90% transmission when unbleached) is placed between the folding mirror and the output coupler at a variable distance X. By varying this distance, the mode size at the saturable absorber changes and hence the condition of saturation. In this way, as the absorber is displaced along the arm of the cavity, different dynamical regimes, such as periodic behavior (periods 2, 4, and 6), a period-three stable window [20], and chaotic regimes with and without EEs [15] are observed. It must be noted that changes in the position X of the saturable absorber do not affect the Fresnel number of the cavity, which remains constant for all the measurements reported in this contribution. Be aware that the series of dynamical regimes that appear as X is varied is repetitive but that the dynamical regime observed for a precise value of X is not. That is, due to hysteresis cycles and sensitivity to small changes in alignment, pump focusing, etc., one should not expect to find an exact and stable correlation between the value of X and the dynamical regime observed.

One of the output beams at the folding mirror is focused into a *p-i-n* fast photodiode (100-ps rise time) connected to a PC oscilloscope (PicoScope 6403B, 500-MHz bandwidth, 5 GS/s, memory of 1 GS). Time series of the self-Q-switching peak pulse intensities with several thousand pulses are recorded. These series are later analyzed with the TISEAN software package [21,22] in order to calculate the dimension of embedding and the Lyapunov exponents. A VGA CCD camera with 60-fps time resolution connected to a PC allows one to record the image of the intensity distribution. The whole setup is mounted on an optical table with interferometric stability.

B. Interferograms

In order to study the transversal coherence of the spot in different dynamical regimes, we use a modified Mach-Zehnder interferometer. The laser beam is collimated with a convergent lens ($F = 100$ mm) placed 90 mm from the output coupler

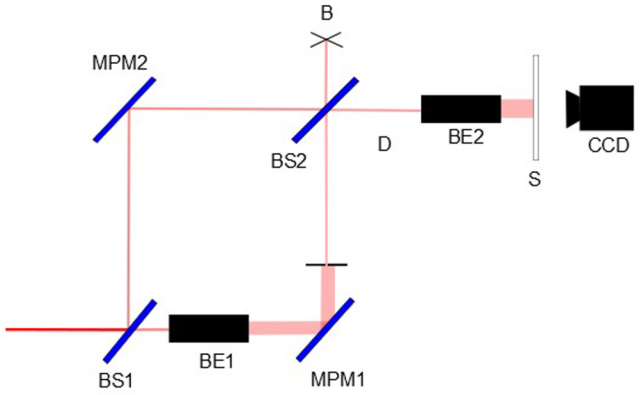

FIG. 2. (Color online) Modified Mach-Zehnder interferometer used to study transversal coherence of the spot. BS1: beam splitter, transmission 96%; MPM1 and MPM2: metallic plane mirrors; BE1 and BE2: 5× beam expanders; BS2: 50/50 beam splitter; D: diaphragm; S: screen; CCD: CCD camera; B: block.

and then directed into the interferometer shown in Fig. 2. The configuration of the Mach-Zehnder is such that it allows us to obtain, by means of a 5× beam expander, a superposition of the spot with a magnified partial section of itself. This output is in turn magnified (so as to make easier the task of discerning interference fringes), projected on a screen, and registered with the CCD camera.

C. Measurement of intensities in partial sections of the spot

The comparison of intensities in different partial sections of the spot (by means of plots of the intensity in one section vs the intensity in the other) is a useful way to study its transverse dynamics in a pulse-to-pulse evolution. It allows us to determine, for example, whether EEs are linked to specific transverse patterns. A complementary approach to characterize the transverse dynamics is the two-point spatial correlation. Unlike the plots of intensities in different sections, it provides a magnitude averaged over a whole time series, and it is useful to identify the presence of spatial domains and eventually detect spatiotemporal chaos.

In order to study these features, a loss beam (see Fig. 1) is magnified with a 5× beam expander and then directed to a 50/50 beam splitter. Both reflected and transmitted beams are then measured with two photodiodes, which are covered by masks with 1-mm-diameter pinholes to limit the measured section, and connected to the PC oscilloscope. One of these photodiodes (which we call photodiode A) is fixed and is kept measuring the center of the spot, while the other (photodiode B) is mounted on a micrometric translation stage so that it can measure the intensity in different regions of the spot. Photodiode B is displaced in every case in the horizontal direction. (We refer to the time series measured with photodiodes A and B as *partial peak intensity time series*.) The intensity of the whole spot is at the same time recorded with the photodiode FP and defines whether a pulse is an EE or not. This scheme allows us to measure, simultaneously, the total intensity of the spot and the intensity in two specific regions.

III. RESULTS

A. Correlation among different regions of the spot

1. Intensity plots in different sections of the spot

We study the evolution of the transverse pattern from pulse to pulse by analyzing pairs of simultaneous partial peak intensity time series in different sections of the spot. We call IA_i (IB_i) the peak intensity measured by photodiode A (B) for the ith pulse of the series and IA (IB) the resulting time series. Figures 3(a)–3(d) show IB_i vs IA_i for different distances d (i.e., horizontal separations) between regions A and B for a regime with EEs. Thick (red online) dots indicate the events that are extreme *in the corresponding total peak intensity time series* measured with photodiode FP (see II C); Fig. 3(e) shows

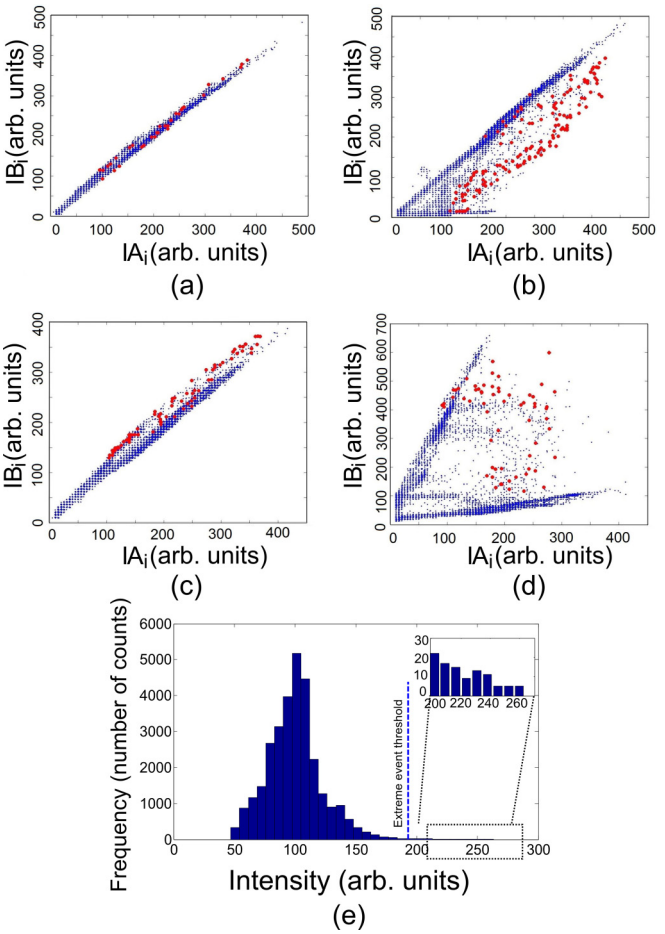

FIG. 3. (Color online) All measurements in the figure are performed for a chaotic regime with extreme events (with a dimension of embedding of 6, and two positive Lyapunov exponents). Position of the saturable absorber $X = 1.7$ cm. (a)–(d) Peak intensity measured in the photodiode B (IB_i) vs peak intensity in photodiode A (IA_i) in arbitrary units such that the average peak intensity for each time series is 100 (the same criterion is used in the rest of the paper), for different values of horizontal separation d: (a) $d = 0$ mm, (b) $d = 1$ mm, (c) $d = 3$ mm, and (d) $d = 8$ mm. Thick (red online) dots indicate extreme events *of the simultaneously recorded total peak intensity time series*. (e) Histogram of peak intensities for a total intensity time trace; the kurtosis of the distribution is 6.02. A zoom of the time trace corresponding to the same data of this histogram is shown in Fig. 4(b), together with the recorded laser spot.

a histogram of the peak intensities for a total intensity time series registered in the same dynamical regime as (a)–(d). In every case, we express the peak intensities in arbitrary units such that the average peak intensity for each time series is 100. We consider this criterion the most appropriate, since it simplifies making comparisons between different dynamical regimes. It is important to note that the three time series (total, IA, IB) are different. Hence, an EE in the total intensity may have, for example, vanishing intensity in IA and/or IB.

As it is expected, for $d = 0$ mm (i.e., when both photodiodes register the same region of the spot), the relation between intensities is linear [see Fig. 3(a)]; for $d = 1$ mm [Fig. 3(b)], the plot spreads, showing an irregular distribution; for $d = 3$ mm [Fig. 3(c)] it becomes practically linear again; and finally, for $d = 8$ mm [Fig. 3(d)] it spreads even more than in the previous case. Four main features arise from these plots: (i) The transverse pattern changes from pulse to pulse in an irregular fashion. (A behavior like this has been reported for periodic regimes of similar systems in Refs. [23,24].) (ii) Some regions of the spot are correlated [e.g., Fig. 3(c)], while others are almost uncorrelated [e.g., Figs. 3(b) and 3(d)]. (iii) EEs appear in different zones of the plots. This implies that the spatial configuration of the spot changes from one EE to another, i.e., the EEs are not associated to a single transverse pattern. Moreover, they occur in a wide range of values both for IA and IB, i.e., some EEs correspond to a high intensity value in section A and low in section B, others to vice versa, and others to a low or high intensity in both sections at the same time. This means that EEs do not occur for a uniformly illuminated pattern and that the more brilliant regions change position from one EE to the other and cannot be associated to a specific location in the transverse pattern. (iv) Despite the seemingly random distribution in (b) and (d), some regularities arise from the plot, e.g., most of the events are contained within two approximately straight lines. This can be interpreted as an indication of the predominance of two different transverse configurations that appear with a higher frequency than the others, but with different total intensities each time.

2. *Spatial correlation*

We calculate the two-point spatial correlation for pairs of peak intensity time series (corresponding to different pairs of sections of the spot). It is defined as

$$C(IA,IB) = \frac{\sum_{i=1}^{N}(IA_i - \overline{IA})(IB_i - \overline{IB})}{\sqrt{\sum_{i=1}^{N}(IA_i - \overline{IA})^2 \sum_{i=1}^{N}(IB_i - \overline{IB})^2}}, \quad (1)$$

where $\overline{IA}$ ($\overline{IB}$) is the average intensity over the whole time series IA (IB).

Figure 4(a) shows the values of $C(IA,IB)$ (as a function of the horizontal separation d between the sections observed by both photodiodes) for two different chaotic regimes with EEs, which we call regime 1 (circles) and regime 2 (squares), and a periodic regime (diamonds). Figures 4(b)–4(d) exhibit both the spots and zooms of the time traces corresponding to these regimes. The different regimes are obtained by adjusting the position of the saturable absorber inside the laser cavity,

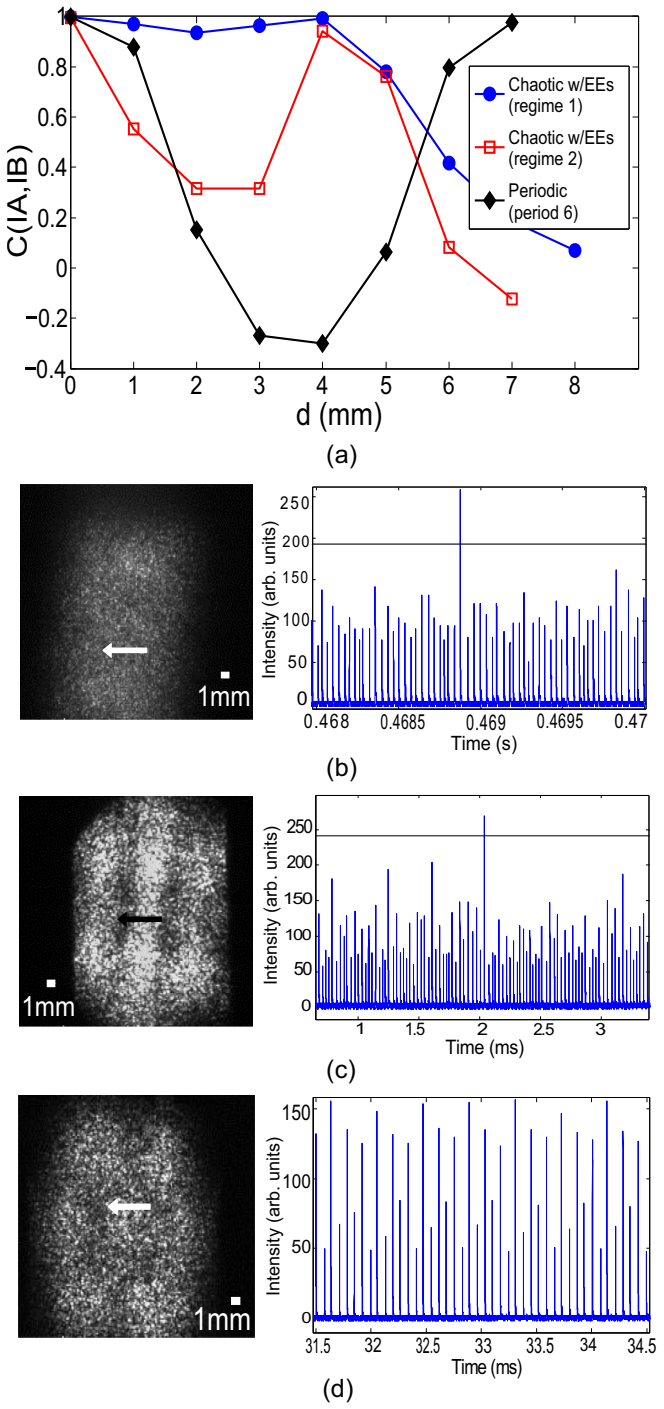

FIG. 4. (Color online) Spatial correlation, spot, and zoom of the time trace for three different dynamical regimes. Regimes 1 ($X = 1.7$) and 2 ($X = 0.5$) are hyperchaotic with extreme events; the third one ($X = 0.65$) is periodic and is shown for comparison. Regime 1 is the same one of Fig. 3. (a) Spatial correlation as a function of the separation d between photodiodes A and B; (b) spot and time trace for regime 1; (c) the same for regime 2; (d) the same for the periodic (period 6) regime. The arrows drawn on the laser spots indicate the initial position ($d = 0$) and direction in which the correlation is measured. The horizontal lines in the time traces in (b) and (c) indicate the extreme event threshold.

as explained in Sec. II A. Regime 1 ($X = 1.7$ cm) is the same that is shown in Fig. 3. Regime 2 ($X = 0.5$ cm) is, as regime 1, hyperchaotic with an embedding dimension of 6 and two positive Lyapunov exponents. The periodic regime ($X = 0.65$ cm) has an embedding dimension of 5, no positive Lyapunov exponents, and period 6.

The line depicted with circles is typical of the regimes with EEs. The coefficient $C(IA, IB)$ remains close to 1 for nearly half the spot radius and then drops to almost 0 near the edge of the spot. This behavior differs from that observed in spatiotemporal chaotic systems with a large number (of the order of several tens) of modes (which can be roughly estimated in optical systems by the Fresnel number), which is characterized by a rapid exponential decay of the correlation [25,26] and/or a narrow peak with a short correlation length [27]. The behavior observed in our laser is consistent, instead, with the existence of a relatively few transverse modes defining domains of correlation that spread through large areas of the spot from pulse to pulse.

Some of the regimes with EEs show a nonmonotonous behavior, such as the one represented by the squares in Fig. 4. This regime has a local peak ≈4 mm away from the center, before decaying for larger d. This does not contradict our previous statement. It implies instead that these regimes are dominated by transverse patterns different from those involved in the aforementioned cases, arguably occupying areas with more complex shapes. This is confirmed by the image of the whole spot registered by the CCD camera.

For comparison, we also show in Fig. 4 the spatial correlation for the case of a periodic regime with period 6 (diamonds). The correlation decays at first, but near the edge of the spot it rises again to a value close to 1. In other periodic regimes, the spatial correlation remains near 1 for almost all of the span of d, except in a few narrow valleys.

B. Time intervals between successive pulses

Figure 5 shows, for a typical chaotic regime with EEs, plots of the intensity of each pulse in the time series against the time interval between that pulse and the previous one ($\Delta t-$, upper graphic), and between that pulse and the next one ($\Delta t+$, lower graphic). The intensity is scaled so that its average value is 100 in arbitrary units. Note that both plots exhibit a remarkable regularity: the width of the range of values of $\Delta t-$ and $\Delta t+$ associated to extreme events is far narrower (roughly 2 and 5 μs, respectively) than that related to, e.g., average pulses (28 and 25 μs). This is most noticeable in the case of $\Delta t-$. This means that (i) if one knows that the next pulse is going to be an EE, then one is able to predict with a precision of ≈1 μs when it is going to occur, and (ii) once an EE has happened, one can predict with a precision of ≈2 μs the time that it takes for the buildup of the next pulse (which is most probably *not* an EE). If an average pulse is considered instead, none of these predictions can be made.

Moreover, the plots provide some hints on the mechanism of generation of EEs. The first one, given by the upper plot, is somewhat counterintuitive: in a simplistic approach, one would expect that the higher the peak intensity, the higher the $\Delta t-$, to allow a longer time to accumulate energy from the pump. However, the $\Delta t-_{\mathrm{EE}}$ (i.e., $\Delta t-$ intervals related to EEs)

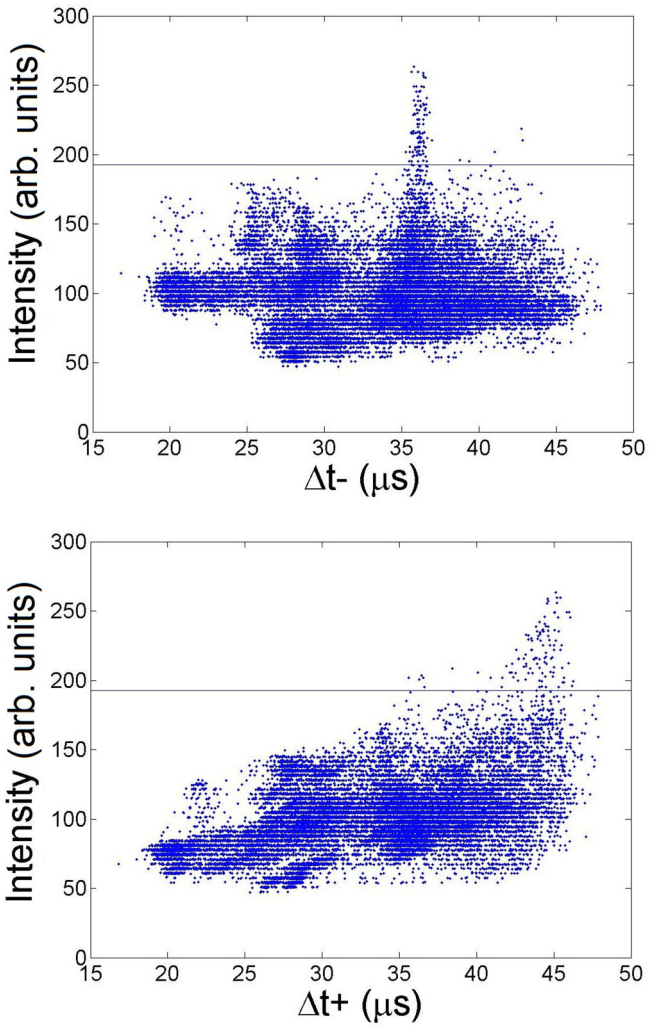

FIG. 5. (Color online) Plots for total peak intensity as a function of interpulse time interval for a chaotic time series with extreme events. The data belong to the time series shown in Fig. 3(e). Upper (lower) figure shows the total peak intensity of as a function of $\Delta t-$ ($\Delta t+$), i.e., the time interval between one pulse and the previous (next) one. The horizontal line indicates the extreme event threshold. Peak intensities are scaled so that an average event has an intensity of 100.

values are not particularly long; in fact, they are closer to the average interval than to the maximum $\Delta t-$, since $\Delta t-_{\mathrm{EE}} \simeq$ 36 μs, while the longest intervals have a value of almost 48 μs. This suggests that an average pulse does not totally deplete the energy available in the gain volume, but instead, it leaves some energy stored in certain regions (possibly due to spatial "hole burning"). This stored energy allows a pulse to reach intensities over the EE threshold, in spite of the relatively short time elapsed since the last one. Therefore, EEs can be thought of as pulses that are more efficient in extracting the energy stored in the gain medium.

The lower plot shows that the range of values of $\Delta t+$ associated to EEs is among the highest of the set, i.e., the time until the next pulse after an EE is always among the longest times that can be expected for a particular time series (typically $\Delta t+ \geqslant 40$ μs, while the average $\Delta t+$ is 33 μs). This means

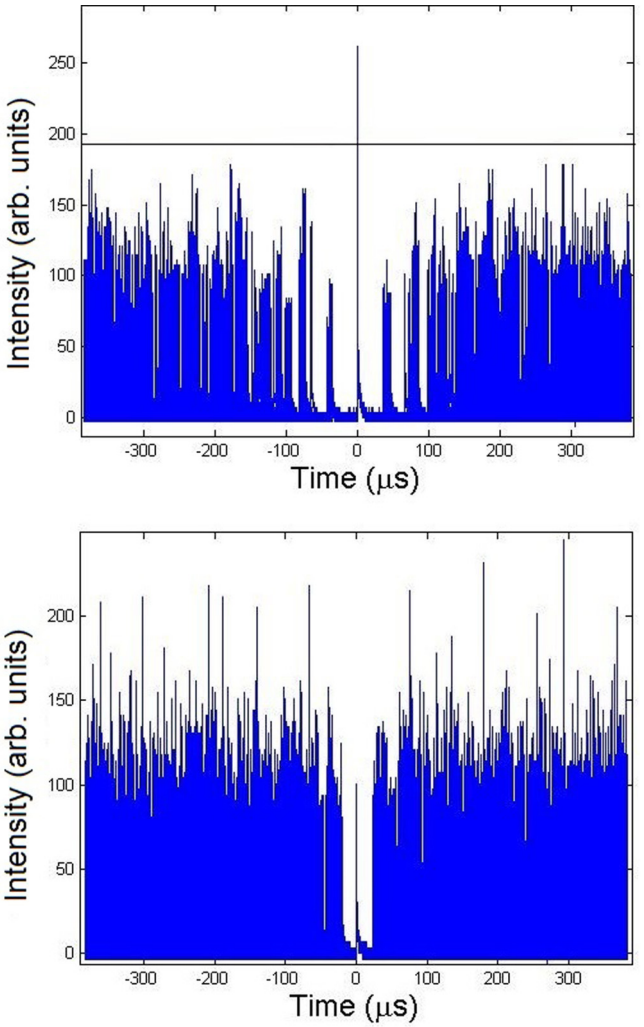

FIG. 6. (Color online) Upper plot: superposition of 112 time traces centered at each of the extreme events of a chaotic regime of operation. The data belong to the same time series whose histogram is shown in Fig. 3(e). The horizontal line shows the extreme event threshold. Lower plot: superposition of time traces centered at 112 near-to-average events for the same time series of the upper plot.

that EEs efficiently deplete the gain so that the time until the next pulse is necessarily long, to allow a new accumulation of gain.

The plots in Fig. 5 show what happens in the immediate vicinity of a given pulse (i.e., one pulse before or one after). Figure 6 exhibits what happens in a larger time scale. It shows, for a time series with 112 EEs, a superposition of time traces centered at each of the EEs (upper plot) and, for comparison, a superposition of the same amount of average pulses (lower plot).[1] Note that all the pulses immediately preceding or following an EE [i.e., if the EE is indexed as the Nth event, these pulses are the $(N+1)$th and $(N-1)$th events] occur within a fairly narrow temporal window that slowly blurs for

[1]Zamora-Munt *et al.* have performed a similar analysis for both experimental and simulated time series of optically injected semiconductor lasers in Ref. [10].

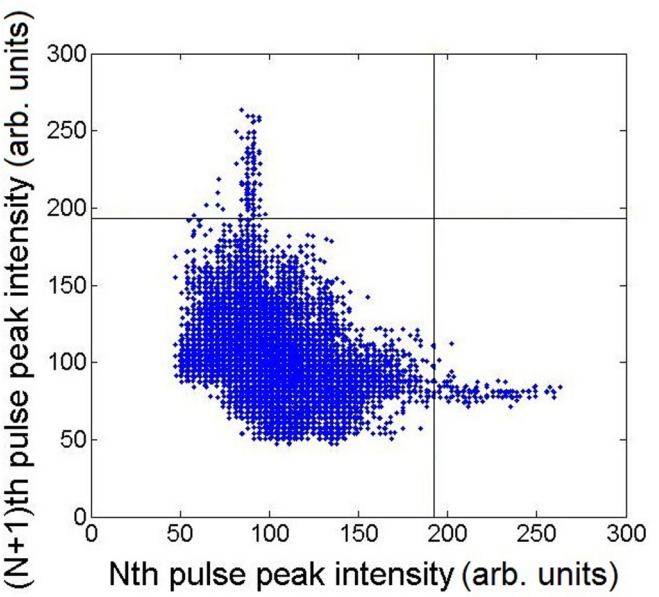

FIG. 7. (Color online) Return intensity map for a chaotic regime of operation with extreme events; the data belong the same time series whose histogram is shown Fig. 3(e). The vertical and horizontal line indicate the extreme event threshold.

farther pulses. [The temporal window in which the $(N+2)$th and $(N-2)$th pulses occur is wider than that of the $(N+1)$th and the $(N-1)$th events, and so on.] On the contrary, for average pulses (lower plot) there is not a regular behavior, even in the immediate vicinity of the pulse. This suggests that the trajectory in phase space corresponding to an EE is confined to a relatively well-defined manifold. This result gives some hope that this type of EE can be predicted with time enough to control them.

C. Return intensity maps

Return maps are plots of a magnitude of the $(N+1)$th vs that of the Nth event in the temporal evolution of a given system. They usually provide useful insight on the dynamics of that system. A return map is shown in Fig. 7 for a chaotic total peak intensities time series with EEs whose histogram is shown in Fig. 3(e). Once again, the EEs exhibit a specific and regular behavior. They appear as two relatively well localized "tongues" emerging from a central bunch at a value of $\simeq$80. (Recall that the average peak pulse intensity is 100 in arbitrary units.) In this case, this means that EEs are preceded and followed by relatively low intensity pulses (slightly below the average), and that the intensity of those pulses is restricted to a narrow range of values. This is consistent to what was shown for EEs in the peak intensity vs interpulse time interval plot of Fig. 5. In other words, the evolution of the peak intensity of the pulses surrounding an EE is quite repetitive. The fact that the pulse preceding the EE is close to average supports the scenario outlined in Sec. III B, in which the pulse prior to an EE fails to totally deplete the gain.

In summary, according to the results presented in Secs. III B and III C, the EEs are not merely high-intensity pulses appearing at random. They seem to follow a more regular

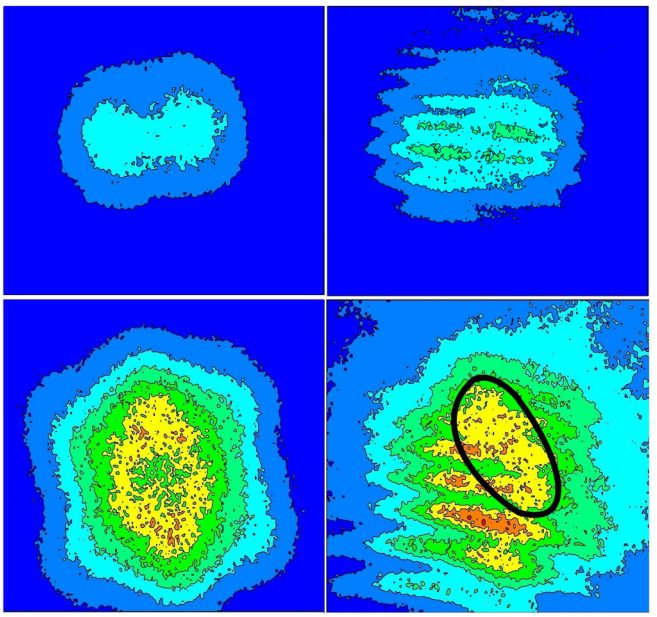

FIG. 8. (Color online) Contour plots of the laser spot and heterodyne interferogram for two different regimes of operation. Upper row: chaotic regime without extreme events (a dimension of embedding of 6, one positive Lyapunov exponent; position of the saturable absorber $X = 0.8$ cm); lower row: chaotic regime with extreme events (a dimension of embedding of 6, two positive Lyapunov exponents; position of the saturable absorber $X = 0.6$ cm); left column: laser spot; right column: interferogram. The region marked with a black line in the lower-right figure indicates where the interference fringes blur.

evolution than that of the average Q-switch pulse. This enforces the idea that there is a deterministic mechanism behind the formation of EEs.

D. Interferograms

Figure 8 shows the contour plots of the laser spots and heterodyne interferograms, obtained as explained in Sec. II B for two different dynamical regimes: a chaotic regime without EEs (upper row) and a chaotic regime with EEs (lower row). In the former regime, fringe patterns are observed all across the spot. In the latter regime, instead, fringes are observed in the region that is expanded on the reference beam and its immediate neighborhood. Outside this region, fringes blur and disappear, indicating that the coherence is lost. It is important to remember that, because the transverse pattern varies from pulse to pulse (as it was shown in Sec. III A 1), and due to the relatively long exposure time of the CCD, neither the spot nor the interferogram correspond to a single pulse transverse pattern but rather to a superposition of many different ones. However, *blurring is not observed in absence of EEs, even if the regime is chaotic*, while it is in the regime with EEs. This result suggests the existence of coherence domains and provides further support to the hypothesis that transverse mode interaction is key in the appearance of EEs in this system. We foresee repeating this experience using an ultrafast camera in order to distinguish pulse-to-pulse spots and interferograms.

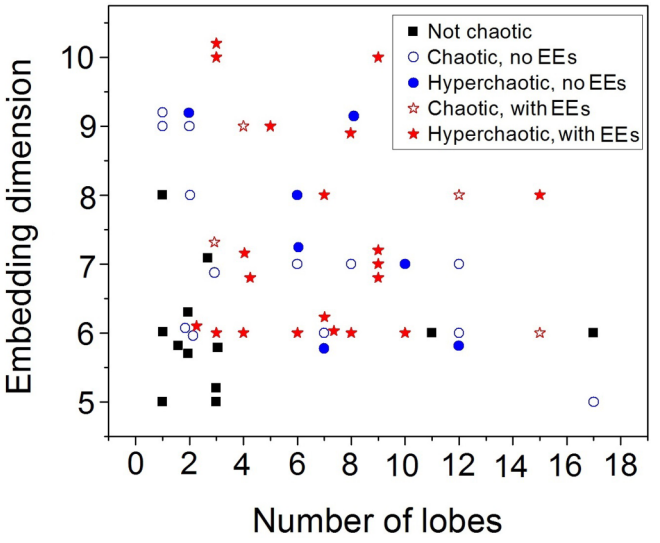

FIG. 9. (Color online) Representation of all the recorded dynamical regimes in this study having a measurable embedding dimension in terms of the number of lobes of their spot (horizontal axis) and their embedding dimension (vertical axis). The shape (and color) code indicates whether the series are not chaotic, i.e., periodic (full, black online, squares), chaotic without extreme events (hollow, blue online, circles), hyperchaotic without extreme events (full, blue online, circles), chaotic with extreme events (hollow, red online, stars) or hyperchaotic with extreme events (full, red online, stars). Noninteger values of embedding dimension must be interpreted as the closest integer value.

E. Dynamical and spatial complexity

Figure 9 summarizes the features of all the time series recorded in this study having a measurable embedding dimension. They are placed according to their spatial complexity, which is quantified by the number of "lobes" in the spot and their value of embedding dimension. Be warned that some of the time series are given a noninteger value of embedding dimension or number of lobes to avoid the superposition of dots and for the sake of clarity; in those cases the embedding dimension or number of lobes must be understood as the closest integer. A shape (and color online) code indicates whether a particular series is nonchaotic, chaotic, hyperchaotic, and whether it displays EEs or not. It can be seen, as a general behavior, that chaotic and hyperchaotic regimes have a large dimension of embedding. Here, "large" means higher than the value of 4 predicted by the standard theoretical model based on rate equations for a single mode [15,16]. The time series with EEs tend to display a large number of lobes, too. This implies that regimes with EEs are associated with a dynamical behavior which is complex both in space and time. On the other hand, chaotic regimes with no EEs and periodic regimes tend to concentrate in the lower-left quadrant of the graph, which implies they have a lower degree of complexity (lower dimension of embedding and spatially simpler spots). This figure enlarges the preliminary results presented in Ref. [20].

IV. SUMMARY

In this paper, we report a series of observations aimed to guide the way to a (still missing) theoretical explanation of the

formation of EEs in all-solid-state, self-Q-switched lasers. In the regimes with EEs, the spatial correlation decays to zero in a distance comparable with the spot size. This is not observed in periodic (therefore without EEs) regimes. No decay associated with a narrow peak is observed as it was, instead, in other extended spatiotemporal systems. This is consistent with the idea that relatively few transverse modes are involved in the formation of the EEs. The plots of the intensities recorded in the two detectors, or IB vs IA, show that the transverse patterns change in an irregular way from pulse to pulse, and that the EEs are not linked to a specific transverse pattern.

From the analysis of the interpulse time intervals we see that (i) the values of $\Delta t-_{\mathrm{EE}}$ ($\Delta t+_{\mathrm{EE}}$) are typically contained in a narrow temporal span, (ii) $\Delta t-_{\mathrm{EE}}$ are next to average, contrary to what might be expected, and (iii) $\Delta t+_{\mathrm{EE}}$, on the other hand, are among the longest interpulse intervals. Result (ii) is consistent with a scenario where typical pulses do not totally deplete the accumulated gain in the active medium but instead leave some energy stored so that the following pulse does not need a build-up time proportional to its intensity. This energy storage is presumably related with spatial hole burning in the active volume. The result (iii) suggests that the deep cause of the EEs is simply that they are particularly efficient in depleting the gain, through a mechanism that is yet to be elucidated. All these results, together with the regular behavior exhibited in Fig. 6, suggest that there exists a deterministic mechanism in the formation of the EEs, and therefore that there is some possibility of predicting and controlling them. The interferograms show the existence of domains of coherence compatible with dynamics ruled by the interaction of a few modes.

Finally, the summarizing diagram in Fig. 9 shows that the EEs are prone to arise in chaotic dynamic regimes with large dimension of embedding and with a spot with a complex transverse structure. This result also supports the few-mode interaction hypothesis as the basis of the mechanism of formation of EEs in this type of lasers.

We foresee using an ultrafast camera in order to record series of individual pulse spots (as well as single-spot interferograms) and identify the ones corresponding to EEs. Another planned course of action is to replace the pump laser diode with a VCSEL, which provides a spatially uniform pump mode, and study its effect on the formation of EEs. Our ultimate goal is the construction of a theoretical model able to predict the dynamics of EEs in this system.

ACKNOWLEDGMENTS

This work was supported by Grant No. FA9550-13-1-0120, "Nonlinear dynamics of self-pulsing all-solid-state laser" of the AFOSR (USA), Contract PIP2011-077, "Desarrollo de láseres sólidos bombeados por diodos y de algunas de sus aplicaciones," of the CONICET (Argentina), Project OPTIROC of the ANR (France), and Project ECOS-Sud: Extreme Events in Nonlinear systems, A14E03 (Argentina-France).

[1] *Extreme Events in Nature and Society*, edited by S. Albeverio, V. Jentsch, and H. Kantz, The Frontiers Collection (Springer, Berlin, 2006).
[2] D. R. Solli, C. Ropers, P. Koonath, and B. Jalali, Nature (London) **450**, 1054 (2007).
[3] J. M. Dudley, F. Dias, M. Erkintalo, and G. Genty, Nat. Photonics **8**, 755 (2014).
[4] V. Ruban, Y. Kodama, M. Ruderman, J. Dudley, R. Grimshaw, P. V. E. McClintock, M. Onorato, C. Kharif, E. Pelinovsky, T. Soomere *et al.*, Eur. Phys. J. Spec. Top. **185**, 5 (2010).
[5] M. Duguay, J. Hansen, and S. Shapiro, IEEE J. Quantum Electron. **6**, 725 (1970).
[6] M. Horowitz, Y. Barad, and Y. Silberberg, Opt. Lett. **22**, 799 (1997).
[7] M. G. Kovalsky and A. A. Hnilo, Phys. Rev. A **70**, 043813 (2004).
[8] S. Residori, U. Bortolozzo, A. Montina, F. Lenzini, and F. T. Arecchi, Fluct. Noise Lett. **11**, 1240014 (2012).
[9] C. Bonatto, M. Feyereisen, S. Barland, M. Giudici, C. Masoller, J. R. Rios Leite, and J. R. Tredicce, Phys. Rev. Lett. **107**, 053901 (2011).
[10] J. Zamora-Munt, B. Garbin, S. Barland, M. Giudici, J. R. Rios Leite, C. Masoller, and J. R. Tredicce, Phys. Rev. A **87**, 035802 (2013).
[11] J. A. Reinoso, J. Zamora-Munt, and C. Masoller, Phys. Rev. E **87**, 062913 (2013).
[12] M. G. Kovalsky, A. A. Hnilo, and J. R. Tredicce, Opt. Lett. **36**, 4449 (2011).
[13] A. A. Hnilo, M. G. Kovalsky, and J. R. Tredicce, in *Proceedings of the Fifth Rio De La Plata Workshop on Laser Dynamics and Nonlinear Photonics* (IEEE, New York, 2011), pp. 1–3.
[14] N. Akhmediev, J. M. Dudley, D. R. Solli, and S. K. Turitsyn, J. Opt. **15**, 060201 (2013).
[15] C. Bonazzola, A. Hnilo, M. Kovalsky, and J. R. Tredicce, J. Opt. **15**, 064004 (2013).
[16] D. Y. Tang, S. P. Ng, L. J. Qin, and X. L. Meng, Opt. Lett. **28**, 325 (2003).
[17] A. E. Siegman, *Lasers* (University Science Books, Sausalito, CA, 1986).
[18] W. Koechner, *Solid-State Laser Engineering*, 6th ed. (Springer, New York, 2006).
[19] A. Yariv, *Quantum Electronics* (John Wiley & Sons, New York, 1975).
[20] C. Bonazzola, A. A. Hnilo, M. G. Kovalsky, and J. Tredicce, in *Proceedings of the "Sixth Rio de la Plata Workshop on Laser Dynamics and Nonlinear Photonics* (IEEE, New York, 2013), pp. 1–3.
[21] T. Hegger, H. Kantz, and T. Schreiber, CHAOS **9**, 413 (1999).
[22] T. Schreiber and A. Schmitz, Physica D **142**, 346 (2000).
[23] M.-D. Wei, Jpn. J. Appl. Phys. **49**, 072701 (2010).
[24] M.-D. Wei, C.-H. Chen, and K.-C. Tu, Opt. Express **12**, 3972 (2004).
[25] F. T. Arecchi, G. Giacomelli, P. L. Ramazza, and S. Residori, Phys. Rev. Lett. **65**, 2531 (1990).
[26] P. C. Hohenberg and B. I. Shraiman, Physica D **37**, 109 (1989).
[27] G. Huyet, M. C. Martinoni, J. R. Tredicce, and S. Rica, Phys. Rev. Lett. **75**, 4027 (1995).